

Topological mapping of space in bat hippocampus

Kentaro Hoffman¹, Andrey Babichev^{1,2} and Yuri Dabaghian^{1,2}

¹*Jan and Dan Duncan Neurological Research Institute,
Baylor College of Medicine, Houston, TX 77030,*

²*Department of Computational and Applied Mathematics, Rice University, Houston, TX 77005*
(Dated: March 6, 2022)

Mammalian hippocampus plays a key role in spatial learning and memory, but the exact nature of the hippocampal representation of space is still being explored. Recently, there has been a fair amount of success in modeling hippocampal spatial maps in rats, assuming a topological perspective on spatial information processing. In this paper, we use the topological model to study 3D learning in bats, which produces several insights into neurophysiological mechanisms of the hippocampal spatial mapping. First, we demonstrate functional importance of the cell assemblies for producing accurate maps of the 3D environments. Second, the model suggests that the readout neurons in these cell assemblies should function as integrators of synaptic inputs, rather than detectors of place cells' coactivity and allows estimating the integration time window. Lastly, the model suggests that, in contrast with relatively slow moving rats, suppressing θ -precession in bats improves the place cells capacity to encode spatial maps, which is consistent with the experimental observations.

I. INTRODUCTION

The principal neurons in mammals' hippocampus—the place cells—fire in discrete locations within the environment—their respective place fields [1, 2]. The spatial layout of the place fields—the place field map—is commonly viewed as a representation of the animal's cognitive map of space, although the exact link between them remains unclear [3]. Experiments in "morphing" 2D environments demonstrate that the place field maps recorded in rats are "flexible": as the environment is deformed, the place fields change their shapes, sizes and locations, while preserving their relative positions [4–7], which suggests that the sequential order of place cells' (co)activity induced by the animal's moves through the place fields remains invariant within a certain range of geometric transformations. Moreover, the temporal patterns of place cell coactivity is preserved [8, 9], which implies that the place cells' spiking encodes a coarse framework of qualitative spatiotemporal relationships, i.e., that the hippocampal map is topological in nature [9–12].

Recently, there appeared a few topological models of the hippocampal map [13–15]. In particular, the approach proposed in [16, 17] allows integrating the local spatial information provided by the individual place cells into a large-scale topological representation of the environment. The idea of such integration is based on the Čech's theorem, according to which the pattern of overlaps between regular spatial domains—the regions— U_1, U_2, \dots, U_N , covering a space X , encodes the topological structure of X [18]. Specifically, the covering regions are used to construct the nerve of the cover, \mathcal{N} —a simplicial complex whose 0D vertices correspond to the covering regions U_i , the 1D links—to pairwise overlaps $U_i \cap U_j$, the 2D facets—to triple overlaps $U_i \cap U_j \cap U_k$ and so forth. The Čech's theorem ascertains that if all of the overlaps between the U_i s are contractible in X , then \mathcal{N} is topologically equivalent to X . An implication is that, if the place fields cover the environment sufficiently densely, then their overlaps should encode its topology. Moreover, since these overlaps are represented by the place cells' coactivities, a similar construction can be carried out in temporal domain [13, 16, 17]: if the animal enters a location in which several place fields overlap, the corresponding place cells produce (with a certain probability) temporally overlapping spike trains, which can be received and processed by the downstream brain areas (Suppl. Fig. 1). In other words, place cells' spiking encodes a "temporal" analogue of \mathcal{N} —a coactivity complex, \mathcal{T} , the vertices of which correspond to active place cells c_i , 1D links—to pairs of coactive cells $[c_i, c_j]$, 2D facets—to coactive triples $[c_i, c_j, c_k]$, etc.

By construction, the coactivity complex incorporates, at any given moment of time t , the entire pool of coactivities produced by the place cell ensemble. Hence, it provides a framework for representing spatial information encoded by the place cells. For example, a sequence of the place cell combinations ignited along a particular path γ corresponds to a sequence of "coactivity simplexes"—a simplicial path Γ that represents γ in \mathcal{T} . It was shown in [16, 17] that if the coactivity complex is sufficiently large (i.e., includes a sufficient number of the coactivity events) and if the parameters of the place cell activity fall into the biological range, then \mathcal{T} correctly captures the topology of the physical environment, \mathcal{E} . For example, a non-contractible simplicial path corresponds to a class of the physical paths that enclose unreachable or yet unexplored parts of the environment. Similarly, two topologically equivalent simplicial paths $\Gamma_1 \sim \Gamma_2$ in \mathcal{T} represent physical paths γ_1 and γ_2 that can be deformed into one another. However, such information is not produced immediately: as the animal begins to navigate a new environment, the coactivity complex \mathcal{T} is small and provides an incomplete and fragmented representation of space; moreover, an undeveloped complex \mathcal{T} typically consists of several disjoint components, each one of which may contain gaps and holes that do not correspond to physically inaccessible spatial domains. As the animal continues to navigate, more combinations of coactive place cells are detected, and the "spurious" gaps disappear, yielding a coactivity complex that faithfully represents the topological structure of the environment. Thus, the progress of spatial learning can be quantified in terms of the evolving coactivity complex's structure, e.g., a list of the holes that it contains at a given moment of time t , or a list of surfaces—loops—that encapsulate these holes [16, 18]. Both the holes and the loops are counted up to topological equivalence. For example, if two such loops can be deformed into one another, then they are counted as different shapes of the same topological object—a topological loop. The number of inequivalent topological loops of a dimensionality n is known as the

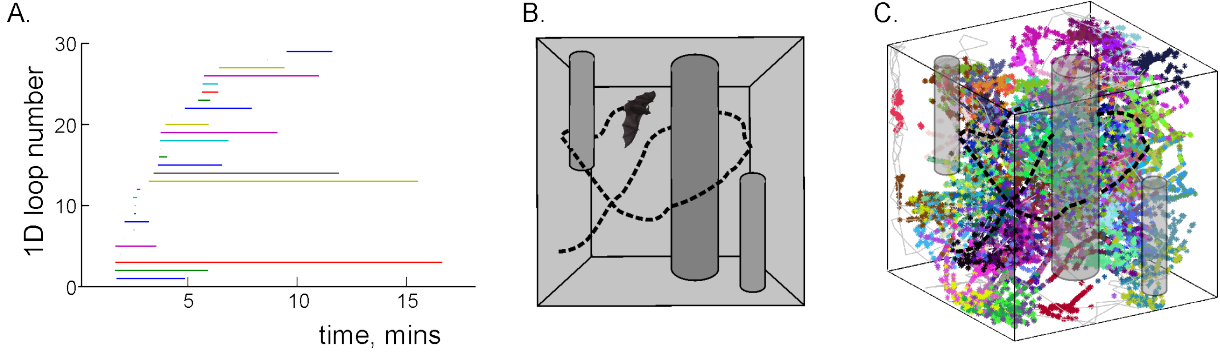


FIG. 1: **Topological map of the bat's environment.** (A) Timelines of 1D loops (colored horizontal lines) encoded in a coactivity complex \mathcal{T} . For as long as a given loop 1D persists, it indicates a noncontractible hole in \mathcal{T} . In this case, the 1D topological loops begin to appear (and hence the holes start to form) in about 2 minutes, and disappear in about 17 minutes, when all the holes in \mathcal{T} close up. (B) A view into a simulated 3D environment ($290 \times 280 \times 270$ cm, sizes taken from [20, 21]) that contains one vertical column and two protrusions—a stalactite hanging over 50 cm from the ceiling, and a 50 cm tall stalagmite. A portion of the simulated trajectory is shown by dashed line. (C) Simulated spikes produced by a virtual bat form 3D spatial clusters—the place fields. Spikes produced by different cells are marked by different colors.

n th Betti number, b_n , and the list of all Betti numbers, (b_0, b_1, b_2, \dots) , provides a convenient “barcode” of the space’s topological structure [19]. Methods of the Persistent Homology theory allow identifying the topological loops in the hippocampal representation of the environment and comparing the resulting Betti numbers $b_n(\mathcal{T})$ with the Betti numbers of the underlying environment, $b_n(\mathcal{E})$. In addition, it is possible to compute the minimal time, T_{\min} , after which the low-dimensional topological structure of \mathcal{T} matches the topology of the environment, which serves as a theoretical estimate of the time required to learn a given space (Figure 1C).

Below we apply this model to investigate spatial learning in bats that learn 3D representations of their environments [20, 21], which produces a number of neurophysiological insights. Specifically, we simulated place cell spiking activity in a bat navigating a small cave with one vertical column and two vertical protrusions, representing a stalactite and a stalagmite (Figure 1A). The topological barcode of this environment is the same as in the 2D open field studied in [16, 17]: $b_0 = 1$ (the cave is connected), $b_1 = 1$ (one 1D topological loop represents paths encircling the column, but not the contractible stalactite and stalagmite) and $b_{n>1} = 0$ (no loops in higher dimensions). However, the increased complexity of the space mapping task elucidates several neurophysiological properties of the hippocampal network that were not explicitly addressed in the previous models.

II. RESULTS

Simplicial coactivity complexes. Our first observation was that, in contrast with the 2D environment in which the correct topological signature emerged in a matter of minutes, the simulated place cell coactivity in 3D failed to represent the cave’s topology. In particular, the first Betti number of the coactivity complex often vanished, $b_1(\mathcal{T}) = 0$, i.e., the place cells did not capture the most salient feature of the navigated space—the central column, although the bat’s trajectory encircled it multiple times.

We reasoned that the discrepancy between $b_1(\mathcal{T})$ and $b_1(\mathcal{E})$ was due to the relatively high speed of the bat’s movements, which caused a mismatch between the temporal pattern of place cell coactivities and the spatial pattern of the place field overlaps. Indeed, if the bat is flying at the speed v , then place cells cofire within a coactivity time window w , even if their place fields are up to $d \approx vw$ apart. If detected by the downstream neurons, these coactivities may lead to an inaccurate representation of space by linking the place cell representations of the physically separated spatial domains. In our simulations, the speed v of the

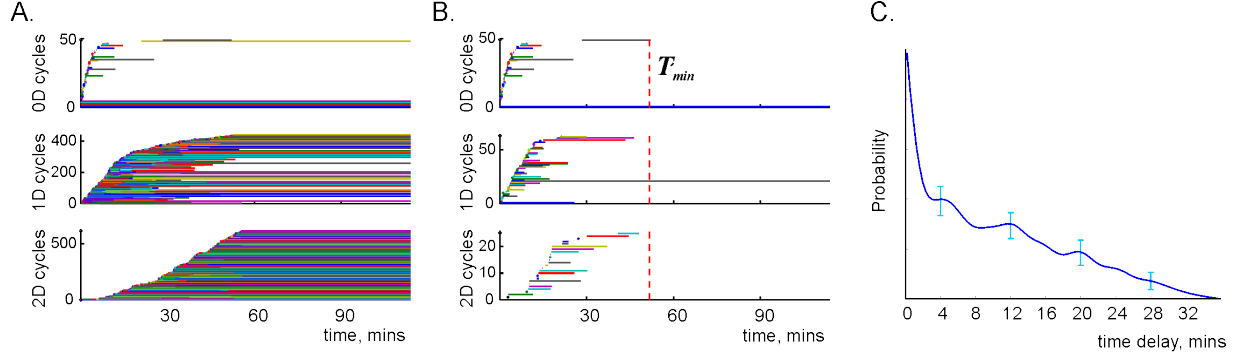


FIG. 2: Learning a topological map by detecting place cell coactivity. (A) A simplicial coactivity complex, built by detecting high order coactivity events, produces large numbers of persisting topological loops in low dimensions. In particular, there are five persistent 0D topological loops (top panel), which implies that hippocampal map of the environment is fragmented in pieces. In addition, there are many persistent loops in 1D (middle panel) which implies that the coactivity complex encodes many noncontractible paths, whereas there is only one class of noncontractible loops in the physical environment. (B) The number of topological loops in the clique coactivity complex is much smaller. In fact, after the $T_{\min} = 28$ minutes (red vertical dashed line), most topological loops disappear, leaving only one topological loop in 0D (which correctly represents the caves connectivity) and one loop in 1D, which represents physical paths circling around the central column. The loops in higher dimensions contract (only the 2D loops are shown, bottom panel), and thus the correct topological barcode ($b_0 = 1, b_1 = 1, b_{n>1} = 0$) emerges. (C) A particular connection may be identified in two ways: either as a clique (completing at t_c , the moment when all the pairs have been accumulated), or simultaneously, as a simplex all cells of which are observed at the moment t_s . The figure shows the probability distribution of the differences between the first appearance times, $\Delta = t_c - t_s$. Since all Δ s are positive, cliques always appear sooner than simplexes.

bat reached at times 2 m/sec, while the place cell inputs were integrated over the coactivity window $w = 0.25$ sec [17, 22, 23]. As a result, place cell coactivities could falsely encode overlaps between place fields that are physically up to 50 cm apart. In particular, place fields across the column may appear “connected,” in which case the column will fail to produce a hole in \mathcal{T} .

Cell assembly constraints. The result outlined above suggests that the pool of place cell coactivities must be additionally constrained to prevent the appearances of “faulty” connections, which, in fact, appeals to well-known neurophysiological phenomenon observed in the hippocampal network. Electrophysiological studies suggest that certain select groups of place cells form functionally interconnected assemblies, which drive their respective “reader-classifier” or “readout” neurons in the downstream networks [25, 26]. Spiking of the readout neurons “actualizes” the information provided by the place cells: if the coactivity of a place cell assembly does not elicit a response of a readout neuron, the corresponding connectivity information does not contribute to the hippocampal map [26]. Thus, a particular selection of the admissible place cell combinations is determined not only by the place coactivities but also by the architecture of the hippocampal cell assembly network, which constrains the pool of place cell coactivities.

It is widely believed that the readout neurons function as “all or none” coactivity detectors, i.e., that they respond to nearly simultaneous activity of the presynaptic cells [26]. Curiously, the topological approach based on the Čech’s theorem corroborates with this point of view: the fact that the nerve complex \mathcal{N} is derived from the spatial overlaps between the regions suggests that a readout neuron should identify these overlaps by detecting nearly simultaneous place cell activity at the times when the animal visits them.

These considerations suggest a simple phenomenological solution to the constraint selection task: to exclude the “spurious” connections, we built the coactivity complex \mathcal{T} , using only the coactivities produced by place cells with the overlapping place fields. However, our subsequent simulations revealed that the cell assembly constraint is too restrictive, because the resulting coactivity complex broke into pieces (on average, $b_0 = 2.3$) and produced a large number of topological loops in 1D and 2D (on average, $b_1 = 36$ and $b_2 = 410$, Figure 2A).

From a biological perspective, this implies that the hippocampal map of the environment remained fragmented and riddled with holes, most of which do not correspond to the actual topological obstacles encountered by the bat. In other words, the simulated cell assembly network, wired to detect place cells coactivities, fails to learn the correct path connectivity of space, which suggests that the system may employ an alternative mechanism of reading out the coactivity information.

Clique coactivity complexes. From a mathematical perspective, the higher order overlaps between regions can be not only empirically detected, but also derived from the lower order overlaps. According to Helly’s theorem [27], a collection of $N > D + 1$ convex regions in D -dimensional Euclidean space will necessarily have a nonempty common intersection if every $D + 1$ of them intersect. For example, a collection of $N \geq 4$ planar regions has a common intersection if any three of them overlap and a collection of $N \geq 5$ regions have a common intersection in $3D$ if any four of them overlap (Suppl. Fig. 2). From the perspective of the Čech’s theorem, this suggests that high-dimensional simplexes in \mathcal{N} can be deduced from their low-dimensional simplexes, which opens new possibilities for constructing coactivity complexes.

Numerical simulations demonstrate that, in fact, the approach of Helly’s theorem can be extended beyond its strict mathematical validity. For example, high order overlaps between place fields in $2D$ environments can be reliably identified by detecting graph-theoretic cliques of pairwise overlaps between them (Suppl. Fig. 2A,B).

Moreover, this information is captured by the place cell coactivity: in the case of the triple place field overlaps, the three pair coactivities, $[c_i, c_j]$, $[c_j, c_k]$ and $[c_i, c_k]$, mark an existing triple overlap of the corresponding place fields in over 90% of cases, and for the higher order overlaps this percent is even higher. This implies that most cliques in the coactivity graph G , defined by the connectivity matrix

$$C_{ij} = \begin{cases} 1 & \text{if cells } c_i, c_j \text{ are coactive and their respective place fields overlap} \\ 0 & \text{otherwise.} \end{cases} \quad (1)$$

correspond to the simplexes of the restricted coactivity complex \mathcal{T} , i.e., that the topological structure of the “clique complex,” \mathcal{T}_{cq} , can approximate the topological structure of \mathcal{T} .

In [28] we demonstrated that in $2D$, the clique coactivity complexes do not only capture the topology of the environment, but often perform better than simplicial coactivity complexes. Similar effects are also observed in the $3D$ case. In our simulations, the number of topological loops in \mathcal{T}_{cq} was much smaller than the number of loops in \mathcal{T} . Moreover, \mathcal{T}_{cq} produced the correct topological signature on average in about $T_{\min} = 28$ minutes—a biologically plausible period of time (Figure 2B).

The success of the clique coactivity complex has a simple intuitive explanation. First, the pairwise coactivities of the place cells are produced when the animal enters the domains where at least two place fields overlap. Since these domains are bigger than the domains of the higher order overlaps (Suppl. Fig. 2C), the pairwise coactivities are produced and detected more reliably than the high-order coactivities. Second, the process of detecting the pairwise coactivities is spread over time. For example, in order to identify a third order coactivity clique, $[c_i, c_j, c_k]$, one can first detect the coactive pair $[c_i, c_j]$, then the pair $[c_j, c_k]$, and then $[c_i, c_k]$, whereas in order to encode a coactivity simplex $[c_i, c_j, c_k]$, all three cells must become active within the same coactivity window w . As shown on Figure 2C, the higher order combinations take longer to appear than the matching collection of pairs—in fact, most coactivity cliques that can be “assembled” over an extended observation process, are never observed as simultaneous coactivity events (Suppl. Fig. 3). This implies that the clique coactivity complex is typically bigger and forms faster, and hence the transient topological loops in \mathcal{T}_{cq} contract sooner.

Integration times. From a physiological perspective, the qualitative difference between the results produced by the “simplicial” and the “clique” approaches to counting the place cell coactivities suggests that the readout networks should build their spiking responses not by detecting rare high-order events, but by integrating low order coactivity inputs. The physiological mechanism for such integration may be based on complex subthreshold summation of the action potentials impinging on the dendritic tree of the readout

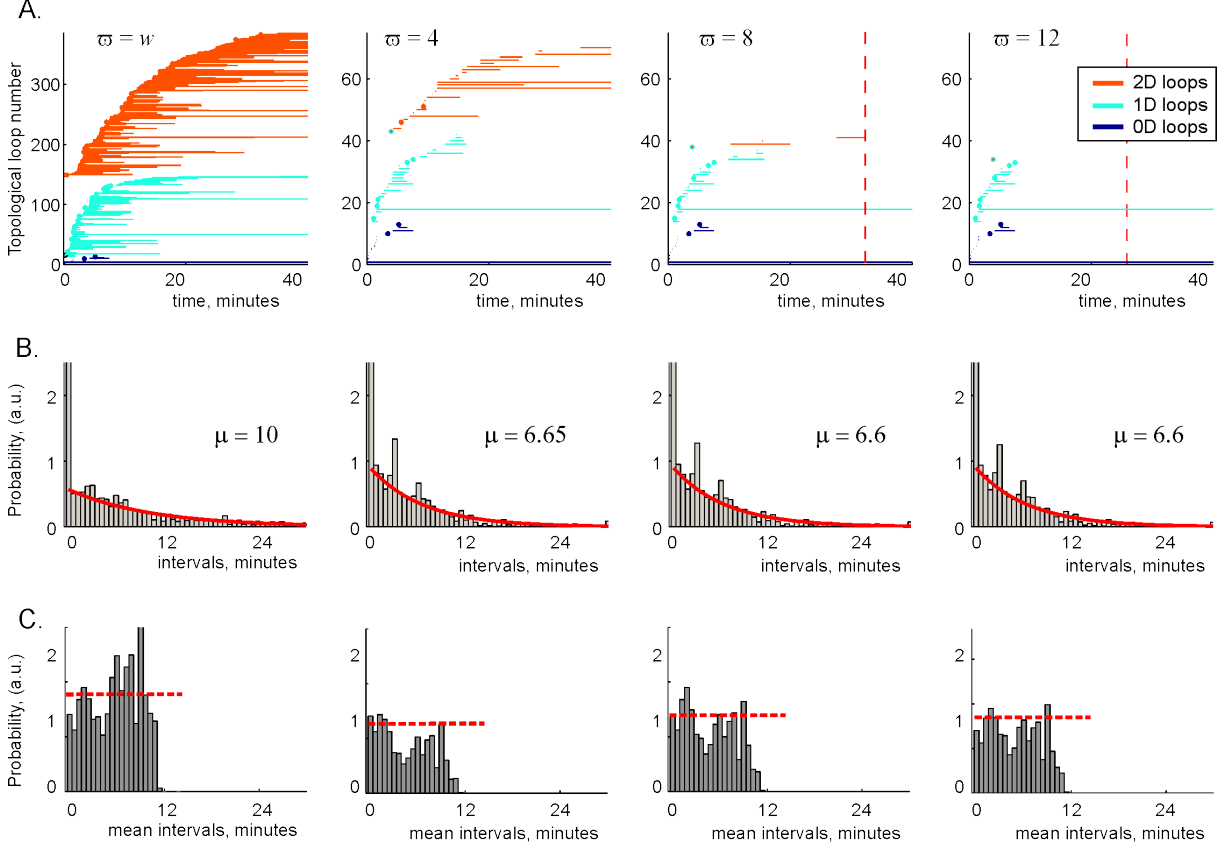


FIG. 3: Timelines of the topological loops in the restricted clique simplicial complexes, obtained for different dendritic integration times. (A) For $\varpi = w$ (in which case the clique complex reduces to the simplicial coactivity complex) spatial learning fails due to numerous spurious topological loops that persist indefinitely in 0D, 1D and in 2D. However, as the dendritic integration time increases to $\varpi = 4$ min, the number of topological loops drops, and only occasional spurious loops remain for $\varpi = 8$ minutes. At $\varpi = 12$ minutes the last 2D loops disappear, and only one persistent loop remains in 1D and 0D after 28 mins, indicating emergence of the correct topological signature. (B) The distribution of the time intervals between the pairs impinging on the readout neurons (see formula (2)). (C) Distribution of the same intervals, averaged for each clique.

neuron. Once a sufficient number of low order coactivity inputs has been received, the readout neuron may produce an action potential, thus actualizing the information about the n th order connection between the regions encoded by the place cells.

Although our modeling approach does not directly address spike integration mechanisms, it allows optimizing parameters in a particular readout algorithm, based on the frequency of the place cell (co)activations produced by the animal's movements through the environment. For example, the model predicts that the coactivity window used by the coincidence detector readout neurons in 2D environments should be about $w \sim 200$ msec wide (smaller w s lead to a rapid increase of the learning times and larger w s lead to instability of learning [17]), which falls into the physiological range of values [22, 23].

What would be then the model's estimate of the time required by the "integrator" neurons to accumulate the place cell coactivities—the clique integration time, ϖ —to produce a complex that reliably represents space? On the one hand, longer clique integration windows allow collecting more coactivities for assembling the cliques, which improves the structure of the coactivity complex (compare Figure 2B and Figure 2A). On the other hand, the larger the ϖ is, the longer the intervals between the consecutive coactivity inputs τ can be, so the information about the presynaptic inputs has to be retained for longer. In contrast, the smaller is ϖ , the tighter the coactivities are "packed" in the integration window. In cases when $\varpi \approx w$, the

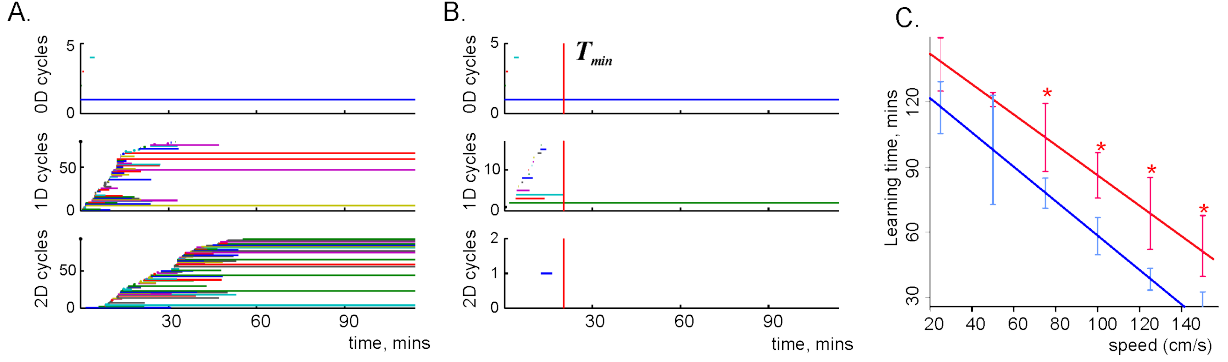


FIG. 4: Suppression of the θ -phase precession improves learning. (A) If the θ -precession in the place cells producing the simplicial coactivity complex is suppressed, then the number of the topological loops in it drops significantly in all dimensions (compare to Figure 2A,B in which θ -precession is present). (B) Similar effect is observed in the clique coactivity complex, if the place cells do not θ -precess. Moreover the learning time $T_{min} = 18$ minutes is smaller than in the θ -precessing place cell ensembles. (C) The average time it took the coactivity complex, \mathcal{T} to converge to a stable signature, as a function of the bat’s mean speed. The times computed for the θ -driven cell assemblies are shown in red and those without θ -precession are colored blue, statistically significant differences are marked by the asterisks over the error bars.

integrator neuron turns into a coincidence detector, and the clique coactivity complex reduces to the simplicial coactivity complex (i.e., when $\varpi \approx \omega$, the results shown on Figure 2B reduce to Figure 2A). By testing several values of ϖ , we found that the place cell map converges if $\varpi \gtrsim 8$ minutes (Figure 3A), making this value the model’s estimate of the clique integration window. Physiologically, this value corresponds naturally to the timescale of working memory (the memory functions responsible for the transient holding, processing and retaining the partial results of learning and memory updating [24]).

We evaluated the combined statistics of the time intervals, τ , between the pairs of action potentials received by the readout neurons within an integration window, across the cell assembly network. As shown on (Figure 3B), the distribution of these intervals consists of two parts: a sharp delta-like peak, $\Delta(\tau)$, concentrated at small values of τ , and an exponential tail,

$$P(\tau) = C_1 \Delta(\tau) + C_2 e^{-\mu\tau}. \quad (2)$$

The exponential rate μ is higher for short ϖ s and decreases towards a stable value of about $\mu \approx 6.6$ minutes as ϖ grows. The fact that building a typical clique requires detecting several coactivities (e.g, a fourth order clique contains six pairwise connections) while mean interval μ between coactivities is comparable to the size of the integration window ϖ , suggests that most coactive inputs are detected “on the spot,” within a small number of consecutive coactivity windows, at the time when the bat crosses a domain where several place fields overlap. This contribution is described by the first part of the distribution, $\Delta(\tau)$, whereas the second part—the exponential tail—represents the connections accumulated over time.

To better understand the statistics of the inputs provided by the cells within the individual cell assemblies we computed, for each ϖ , the mean inter-activity interval, $\bar{\tau}_\sigma$, for each clique σ and studied the statistics of these values. The results shown on (Figure 3C) suggest that the mean inter-activity intervals are distributed much more uniformly, i.e., the population of cell assemblies in which the coactivity integration occurs rapidly is about the same as the population of assemblies that take intermediate or longer times to integrate inputs.

Theta precession is a coupling between the timing of neuronal spikes and the phase of the theta (θ , 4-12 Hz) component of the extracellular field potential, observed in the rat’s hippocampus. As the rat proceeds through a place field, the corresponding place cell spikes at progressively earlier phases of θ -oscillations [29, 30]. This phenomenon produces a strong effect on rats’ spatial learning [31]: suppressing θ -precession with cannabinoids correlates with reduced ability to solve spatial tasks and poorer spatial memory [32, 33].

In contrast, θ -precession in bats is not clearly manifested: according to [34], less than 4% of the bat’s place cells exhibit significant θ -modulated firing.

From a biological perspective, the functional importance of θ -precession for rats navigating 2D environments and lack of thereof in bats navigating 3D spaces might suggest that in the latter case, θ -precession may not produce a similar positive effect on spatial learning. To test this hypothesis, we numerically suppressed the θ -precession in the simulated place cells, which lead to a noticeable decrease of the number of spurious topological loops both in the simplicial and in the clique coactivity complexes (Figure 4). Second, the learning time produced by the clique complex, $T_{\min} = 18$ minutes, became shorter than in the θ -driven coactivity complex.

To explain these results, we reasoned as follows. One can view the effect of θ -precession from two perspectives: on the one hand, it synchronizes place cells’ spiking and hence increases their coactivity rate [29, 30], which speeds up map learning. On the other hand, the fact that the place cells can spike only at specific phases of θ can be viewed as a constraint that reduces the probability of cells’ spiking at every given moment. In [17] we demonstrated that in relatively slow moving rats, the probability of producing spikes during a typical passage through the place field is sufficiently high despite the θ -constraint, so that the main effect of θ -oscillations is spike-synchronization. In contrast, the results of Figure 4 suggest that in bats, the place cells have time to produce only a few spikes during a high speed flight through the 3D place fields, so that the θ -precession only further reduces the cells’ chances of being (co)active.

We tested these results by simulating bat’s movements at different mean speeds: (25, 50, 75, 100, 125, and 150 cm/sec). For each case, 10 simulations were conducted using θ -precessing place cells and 10 simulations with the θ -precession turned off. The results on the Figure 4C show that at no point θ -on ensembles learned faster than the θ -off ensembles: average time until a stable signature was reached in the θ -off case was about 30% less than the time required by the θ -modulated place cell ensembles.

III. DISCUSSION

The topological model of the place cell map of space proposed in [16, 17] provides a framework for bringing together different scales of spatial learning: the macroscale, i.e., the topological and geometrical parameters of the encoded loops, paths, holes, and the microscale, i.e., the parameters of the hippocampal network’s neurophysiology. Applying this model to describe a bat navigating a 3D space reveals several interrelationships between these scales that are implicit in the 2D case, but which have a number of important physiological implications.

First, the failure of the naïve counting of the place cell cofirings indicates a functional necessity of “thinning out” the pool of coactivities using a cell assembly network. Qualitatively, this result is based on simple observation: if the readout neurons respond unrestrictedly to the place cell coactivities then the animal’s rapid moves across the environment will necessarily encode false connections between remote spatial regions, which will result in an incorrect map of space. Second, a striking difference between the simplicial and the clique complexes’ ability to capture the topology of the 3D environment suggests that the information about the high order spatial relationships should be deduced from low order coactivity events, rather than instantaneously detected. The qualitative reasons for this effect are also transparent: the high order coactivity events, represented by the simplexes, are rarer and harder to detect than the matching collections of pairwise coactivities, represented by the cliques. Third, the amount of time over which readout neurons integrate inputs should be longer than observed in previous computational or in vitro studies, in which neurons were studied individually and independently from the task solved by the net neuronal ensemble [35–40]. In contrast, our approach provides a basic contextual description of neuronal activity: the frequency with which the place cells’ action potentials impinge on the readout neuron depends on the frequency of the animal’s visits to specific spatial locations. This frequency would not change significantly if the number of simulated place cells would increase, which suggests that our estimates of the “clique inte-

gration windows” ϖ may give a correct qualitative estimate of the physiological dendritic integration times required by the downstream networks.

Lastly, the model provides a functional insight into why the θ -precession is physiologically suppressed in bats’ hippocampi. Thus, our model provides an example of a “top-down” approach, in which neurophysiological properties of the network are deduced from the task solved by the network.

IV. METHODS

The navigational parameters: the mean speed of the bat ($v_{\text{mean}} = 66$ cm/s, $v_{\text{max}} = 150$ cm/s), and the dimensions of the environment ($290 \times 280 \times 270$ cm) were taken from [21]. For increased reliability of the results, the duration of the navigation session (120 min) was longer than reported in [21].

Place fields. The centers of the place fields, $r_c = (x_c, y_c, z_c)$, were uniformly distributed over the environment, to simulate non-preferential representation of locations. Given the typical sizes of the place fields ($L_c = 95$ cm), the size of the simulated place cell ensemble was chosen to create enough 2D and 3D simplexes in the coactivity complex, sufficient to build a 3D map. Computationally, we could afford about seven place fields per dimension, i.e., $N_c = 343$ place cells total, which corresponds to about $N_c = 50$ cells in a the planar 1×1 m environment studied in [16, 17]. The Poisson spiking rate of a place cell c at a point $r(t) = (x(t), y(t), z(t))$ is

$$\lambda_c(r) = f_c e^{-\frac{(r-r_c)^2}{2s_c^2}}. \quad (3)$$

The peak firing rates f_c of different cells were log-normally distributed around the typical experimental value, $f = 8$ Hz and $s_c = L_c/3$ [21].

θ -phase precession. As the animal enters the field of a cell c , and moves over a distance l towards the center, the preferred spiking phase is $\varphi_{\theta,c} \approx 2\pi(1 - l/L_c)$ [30, 41]. To simulate the coupling between the firing rate and the θ -phase, we modulated the original Gaussian firing rate by a θ -factor $\Lambda_{\theta,c}(\varphi)$,

$$\Lambda_{\theta,c} = e^{-\frac{(\varphi - \varphi_{\theta,c})^2}{2\varepsilon_c^2}}. \quad (4)$$

The width, ε , of the Gaussian was defined in [17], as the ratio of the mean distance that the animal travels during one θ -cycle to the size of the place field, $\varepsilon = 2\pi v/L\omega_\theta$, where v is the rat’s speed and $\omega_\theta/2\pi$ is the frequency of the θ -signal.

Cell assembly constraint. The functional connectivity between place cells in the hippocampal network is described by a graph G , the vertices of which correspond to the active place cells and links to coactive pairs, restricted by the constraints (see formula (1)). The connectivity matrix A_{ij} of G is defined as follows. First, we define the relational matrix C_{ij} : $C_{ij} = 1$ if the cells c_i and c_j exhibit coactivity during the navigation period and $C_{ij} = 0$ otherwise. The place field map’s connectivity matrix, P_{ij} , is based on the place fields’ spatial overlap: $P_{ij} = 1$ if the distance between the place field centers is smaller than the sum of their half-sizes, $d(c_i, c_j) \leq (L_i + L_j)/2$, and $P_{ij} = 0$ otherwise. In principle, the matrix P_{ij} can be deduced directly from the temporal pattern of place cell coactivity [28]; however we used the place field information to simplify our analyses. To constrain the pool of coactivities by the place field map structure, we used the Hadamard product, $A_{ij} = C_{ij}P_{ij}$. The simplexes of the clique coactivity complex, \mathcal{T}_{cq} , correspond to “cliques” of the relational graph G .

Coactivity. A group of cells c_1, c_2, \dots, c_n , counts as coactive, if each one of them fires at least two spikes within the coactivity window $w \approx 250$ msec, i.e., in less than two θ -periods. In [17] we demonstrated this value of w is optimal both in presence and in absence of the θ -precession.

V. ACKNOWLEDGMENTS

The work was supported in part by Houston Bioinformatics Endowment Fund, the W. M. Keck Foundation grant for pioneering research and by the NSF 1422438 grant.

VI. REFERENCES

- [1] O'Keefe J, Dostrovsky J (1971) The hippocampus as a spatial map. Preliminary evidence from unit activity in the freely-moving rat, *Brain Res*, 34, pp. 171-175.
- [2] Best PJ, White AM, Minai A (2001) Spatial processing in the brain: the activity of hippocampal place cells, *Annu Rev Neurosci.*, 24, pp. 459-486.
- [3] O'Keefe J, Nadel L (1978) *The hippocampus as a cognitive map*, New York: Clarendon Press; Oxford University Press. xiv, 570 pp.
- [4] Gothard KM, Skaggs WE, McNaughton BL (1996) Dynamics of mismatch correction in the hippocampal ensemble code for space: interaction between path integration and environmental cues, *J Neurosci.*, 16, pp. 8027-8040.
- [5] Leutgeb JK, Leutgeb S, Treves A, Meyer R, Barnes CA, et al. (2005) Progressive transformation of hippocampal neuronal representations in "morphed" environments, *Neuron*, 48, pp. 345-358.
- [6] Wills TJ, Lever C, Cacucci F, Burgess N, O'Keefe J (2005) Attractor dynamics in the hippocampal representation of the local environment, *Science*, 308, pp. 873-876.
- [7] Touretzky DS, Weisman WE, Fuhs MC, Skaggs WE, Fenton AA, et al. (2005) Deforming the hippocampal map, *Hippocampus*, 15, pp. 41-55.
- [8] Diba K, Buzsaki G (2008) Hippocampal network dynamics constrain the time lag between pyramidal cells across modified environments, *J Neurosci.*, 28, pp. 13448-13456.
- [9] Dabaghian Y, Brandt VL, Frank LM (2014) Reconceiving the hippocampal map as a topological template, *eLife* 10.7554/eLife.03476.
- [10] Alvernhe A, Sargolini F, Poucet B (2012) Rats build and update topological representations through exploration, *Anim. Cogn.*, 15, pp. 359-368.
- [11] Poucet B, Herrmann T (2001) Exploratory patterns of rats on a complex maze provide evidence for topological coding, *Behav. Processes*, 53, pp. 155-162.
- [12] , Wu X, Foster DJ (2014) Hippocampal Replay Captures the Unique Topological Structure of a Novel Environment, *J Neurosci.*, 34, pp. 6459-6469.
- [13] Curto C, Itskov V (2008) Cell groups reveal structure of stimulus space, *PLoS Comput. Biol.*, 4, e1000205.
- [14] Chen Z, Gomperts SN, Yamamoto J, Wilson MA (2014) Neural representation of spatial topology in the rodent hippocampus, *Neural Comput.*, 26, pp. 1-39.
- [15] Chen Z, Kloosterman F, Brown E, Wilson M (2012) Uncovering spatial topology represented by rat hippocampal population neuronal codes, *J Comput. Neurosci.*, 33, pp. 227-255.
- [16] Dabaghian Y, Mmoli F, Frank L, Carlsson G (2012) A Topological Paradigm for Hippocampal Spatial Map Formation Using Persistent Homology, *PLoS Comput. Bio.*, 8: e1002581.
- [17] Arai M, Brandt V, Dabaghian Y (2014) The Effects of Theta Precession on Spatial Learning and Simplicial Complex Dynamics in a Topological Model of the Hippocampal Spatial Map, *PLoS Comput. Biol.*, 10: e1003651.
- [18] Hatcher A (2002) *Algebraic topology*, Cambridge; New York: Cambridge University Press.
- [19] Ghrist R (2008) Barcodes: The persistent topology of data, *Bulletin of the American Mathematical Society*, 45, pp. 61-75.
- [20] Ulanovsky N, Moss CF (2007) Hippocampal cellular and network activity in freely moving echolocating bats, *Nat. Neurosci.*, 10: pp. 224-233.
- [21] Yartsev MM, Ulanovsky N (2013) Representation of Three-Dimensional Space in the Hippocampus of Flying Bats, *Science*, 340, pp. 367-372.
- [22] Mizuseki K, Sirota A, Pastalkova E, Buzsaki G (2009) Theta oscillations provide temporal windows for local circuit computation in the entorhinal-hippocampal loop, *Neuron*, 64, pp. 267-280.
- [23] Huhn Z, Orbn G, rdi P, Lengyel M (2005) Theta oscillation-coupled dendritic spiking integrates inputs on a long time scale, *Hippocampus*, 15, pp. 950-962.
- [24] Goldman-Rakic PS (1995) Cellular basis of working memory, *Neuron* 14: 477-485.
- [25] Harris KD, Csicsvari J, Hirase H, Dragoi G, Buzsaki G (2003) Organization of cell assemblies in the hippocampus, *Nature*, 424, pp. 552-556.
- [26] Buzsaki G (2010) Neural syntax: cell assemblies, synapsembles, and readers, *Neuron*, 68, pp. 362-385.

- [27] Avis D, Houle ME (1995) Computational aspects of Helly's theorem and its relatives, *International Journal of Computational Geometry & Applications*, 05, pp. 357-367.
- [28] Babichev A, Memoli F, Ji D, Dabaghian Y (2015) Combinatorics of Place Cell Coactivity and Hippocampal Maps. *in submission*; arXiv:1509.01677).
- [29] Skaggs WE, McNaughton BL, Wilson MA, Barnes CA (1996) Theta phase precession in hippocampal neuronal populations and the compression of temporal sequences, *Hippocampus*, 6, pp. 149-172.
- [30] Buzsaki G (2002) Theta oscillations in the hippocampus, *Neuron*, 33, pp. 325-340.
- [31] Buzsaki G (2005) Theta rhythm of navigation: link between path integration and landmark navigation, episodic and semantic memory, *Hippocampus*, 15, pp. 827-840.
- [32] Robbe D, Buzsaki G (2009) Alteration of theta timescale dynamics of hippocampal place cells by a cannabinoid is associated with memory impairment, *J Neurosci.*, 29, pp. 12597-12605.
- [33] Robbe D, Montgomery SM, Thome A, Rueda-Orozco PE, McNaughton BL, et al. (2006) Cannabinoids reveal importance of spike timing coordination in hippocampal function, *Nat Neurosci.*, 9, pp. 1526-1533.
- [34] Heys JG, MacLeod KM, Moss CF, Hasselmo ME (2013) Bat and Rat Neurons Differ in Theta-Frequency Resonance Despite Similar Coding of Space, *Science*, 340, pp. 363-367.
- [35] London M, Husser M (2005) Dendritic Computation, *Annu Rev. Neurosci.*, 28, pp. 503-532.
- [36] Brody CD, Romo R, Kepecs A (2003) Basic mechanisms for graded persistent activity: discrete attractors, continuous attractors, and dynamic representations, *Curr. Opin. Neurobiol.*, 13, pp. 204-211.
- [37] Magee JC (2000) Dendritic integration of excitatory synaptic input, *Nat. Rev. Neurosci.*, 1, pp. 181-190.
- [38] Spruston N (2008) Pyramidal neurons: dendritic structure and synaptic integration, *Nat. Rev. Neurosci.*, 9, pp. 206-221.
- [39] Rall W (1989) Cable theory for dendritic neurons. In: Christof K, Idan S, editors. *Methods in neuronal modeling*, MIT Press. pp. 9-92.
- [40] Jarsky T, Roxin A, Kath WL, Spruston N (2005) Conditional dendritic spike propagation following distal synaptic activation of hippocampal CA1 pyramidal neurons, *Nat. Neurosci.*, 8, pp. 1667-1676.
- [41] Huxter JR, Senior TJ, Allen K, Csicsvari J (2008) Theta phase-specific codes for two-dimensional position, trajectory and heading in the hippocampus, *Nat. Neurosci.*, 11, pp. 587-594.

VII. SUPPLEMENTARY FIGURES

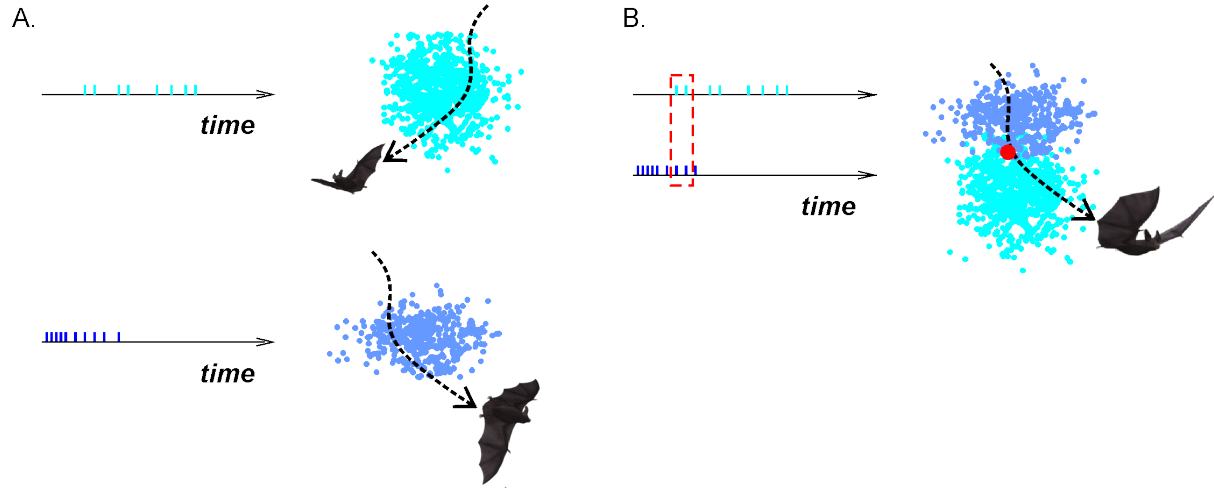


FIG. S1: **Spatial overlap encoded by temporal coactivity.** (A) Place cells produce spike trains as the bat is flying through their respective place fields. (B) Coactivity of two cells (indicated by the dashed box) marks the domain where two place fields overlap.

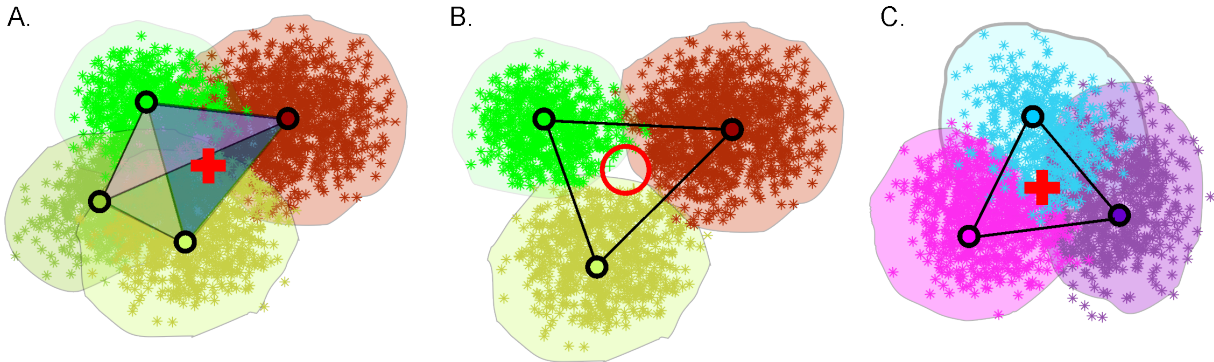


FIG. S2: **A 2D illustration of Helly's theorem.** (A) If every three out of four convex planar regions overlap each other, then they necessarily have a common fourth order overlap, marked by the red cross. (B) For three regions, pairwise overlappings may not yield a common third order intersection—the hollow spot in the middle is marked by the red circle. However, this configuration is statistically rare. (C) Typically, a set of three pairwise overlapping regions is a reliable signature of a triple overlap. In other words, a 2D clique almost always is a 2D simplex (and any simplex is always a clique).

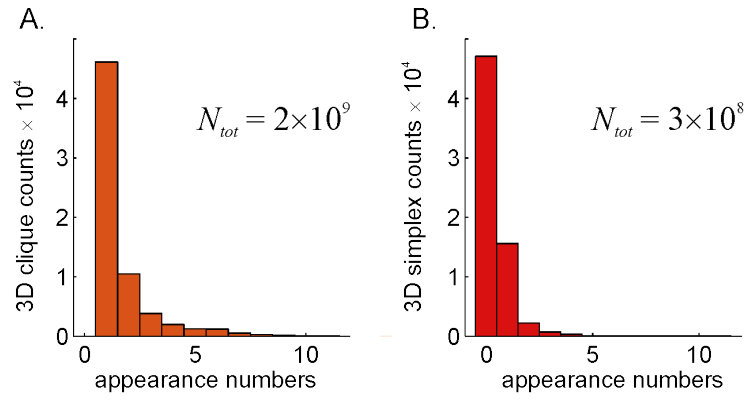


FIG. S3: **The histograms of appearance numbers of 3D cliques (A) and 3D simplexes (B).** Note that the highest occupancy bin on the right panel corresponds to zero appearance rate, i.e., most configurations that observed as cliques, never appear as simplexes, and as a result the total number N_{tot} of cliques and simplexes differ by an order of magnitude.